Supplementary Materials for

Monolayer Tellurenyne assembled with Helical Telluryne: Structure and Transport Property

Liujian Qi, Jie Han, Wang Gao,* and Qing Jiang*

Key Laboratory of Automobile Materials, Ministry of Education, Department of Materials Science and Engineering, Jilin University 130022, Changchun, China.
*Corresponding author. Email: wgao@jlu.edu.cn; jiangq@jlu.edu.cn.

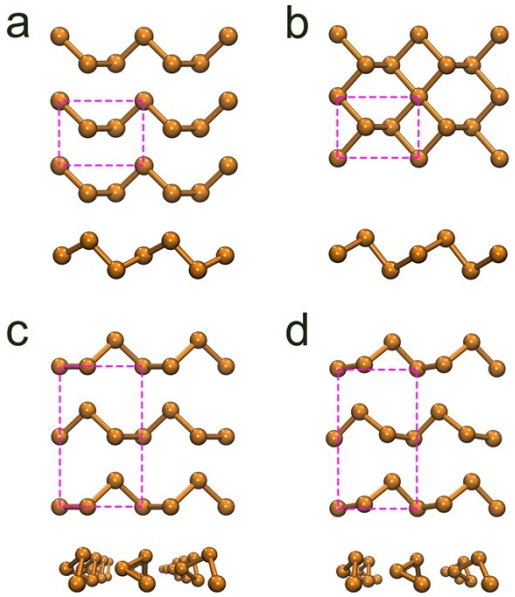

Figure S1. Atomic structures of monolayer Te and tellurenyne. Monolayer Te directly from the bulk phase before (a) and after geometry optimization (b). Tellurenyne (phase I for example) consisting of left-handed and right-handed chains before (c) and after geometry optimization (d). The pink dashed lines represent the unit cell. The side views are shown below the top views.

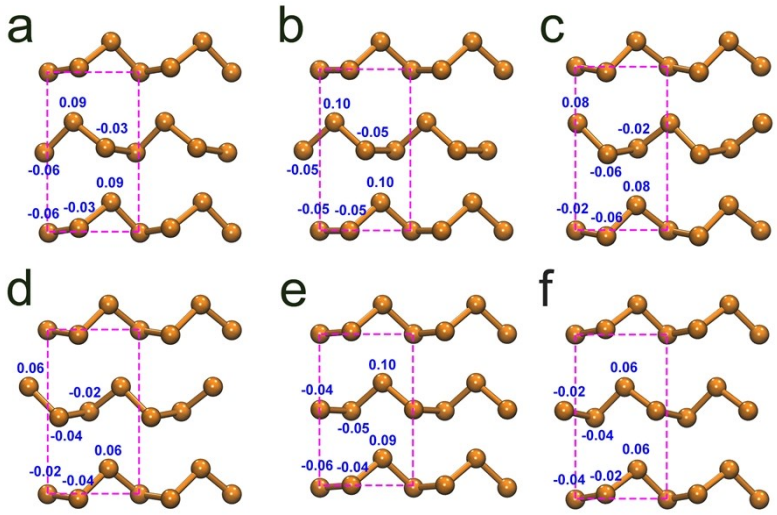

Figure S2. Top views of the six different tellurenyne phases. The corresponding Mulliken charge distribution of Te atoms are labeled. Figures (a)-(f) represent the phases from I to VI.

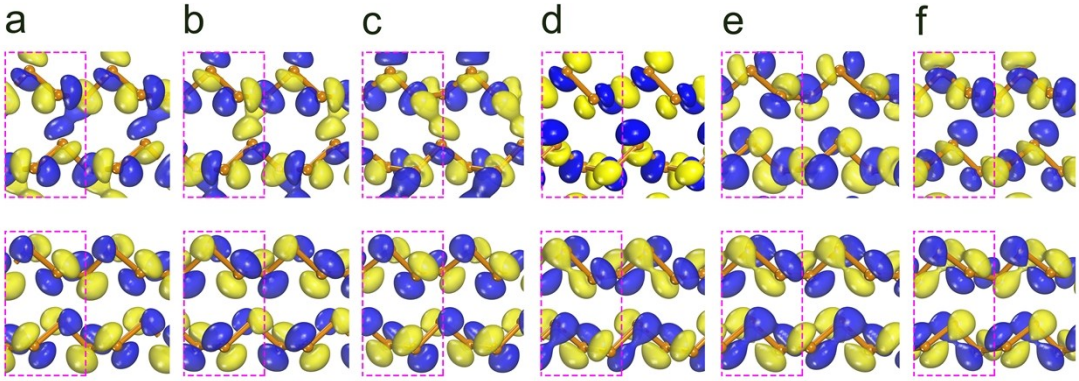

Figure S3. HOMO and LUMO orbits of the six different tellurenyne phases. The upper and down parts represent LUMO and HOMO orbits, respectively. Figures (a)-(f) represent the phases from I to VI.

Table S1. The contribution of electrostatic interactions (E_e) to the binding energy in meV/atom for the six different tellurenyne phases.

	I	II	III	IV	V	VI
E_e	632.77	720.64	548.04	539.08	686.27	532.51

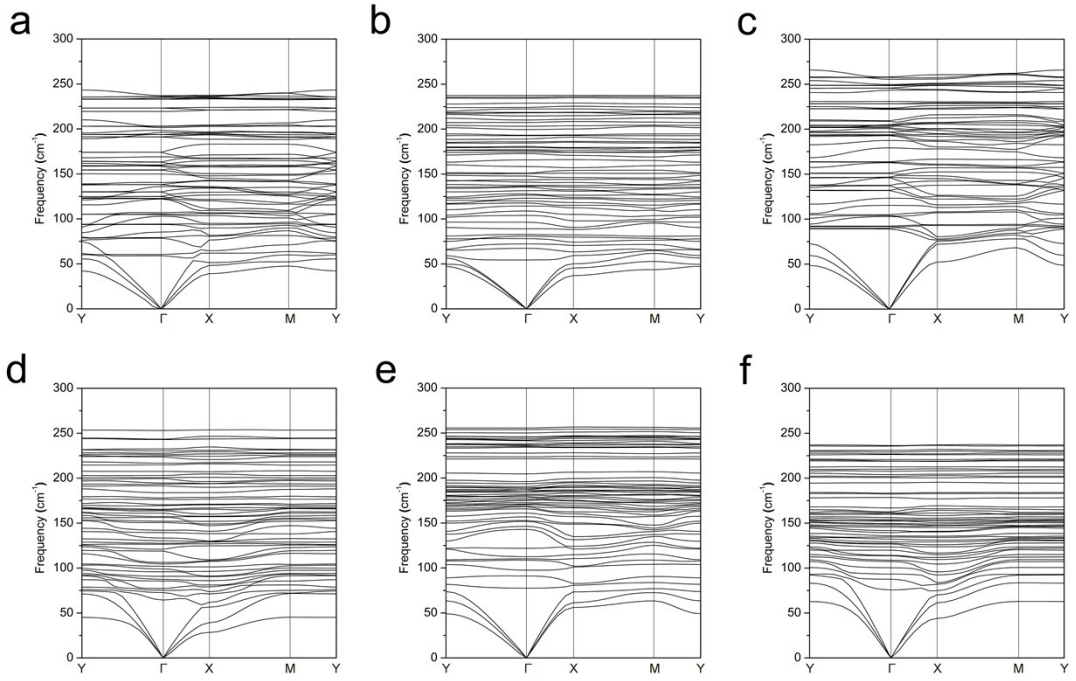

Figure S4. Phonon dispersion of the six different tellurenyne phases. Figures (a)-(f) represent the phases from I to VI.

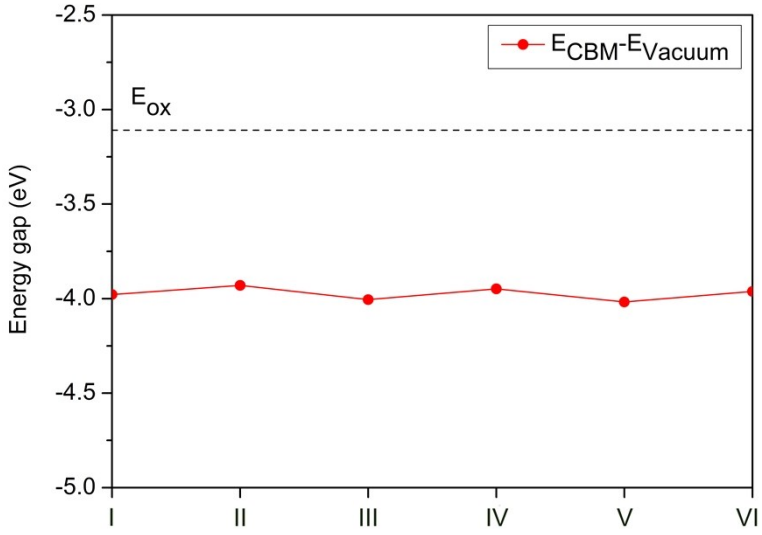

Figure S5. Energy diagrams of conduction band edges of the six different tellurenyne phases. E_{ox} represents the energy diagram of the densities of states of aqueous oxygen acceptor.

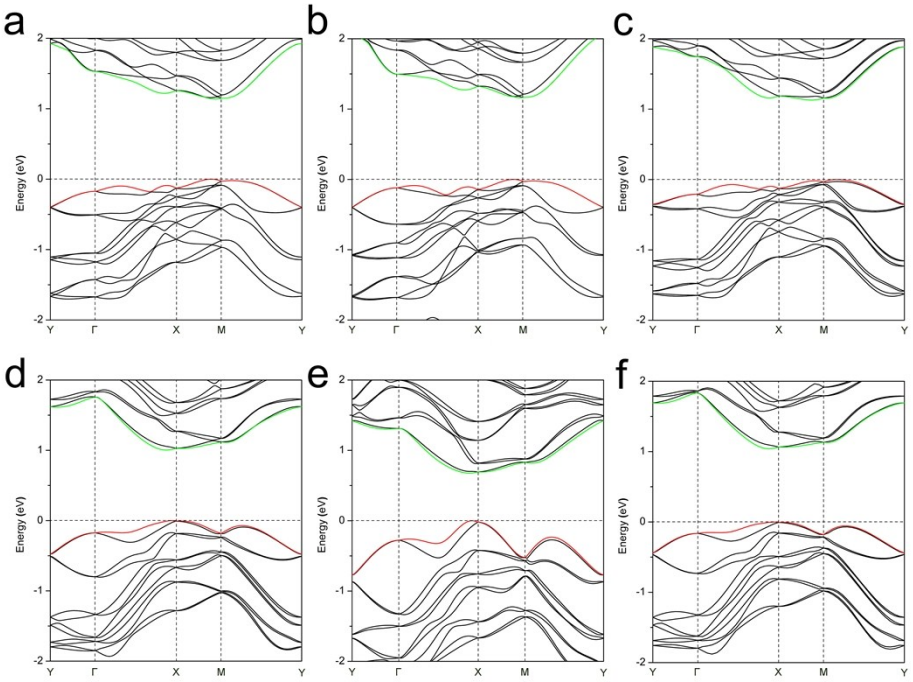

Figure S6. Band structures of the six different tellurenyne phases (PBE+SOC results). Figures (a)-(f) represent the phases from I to VI.

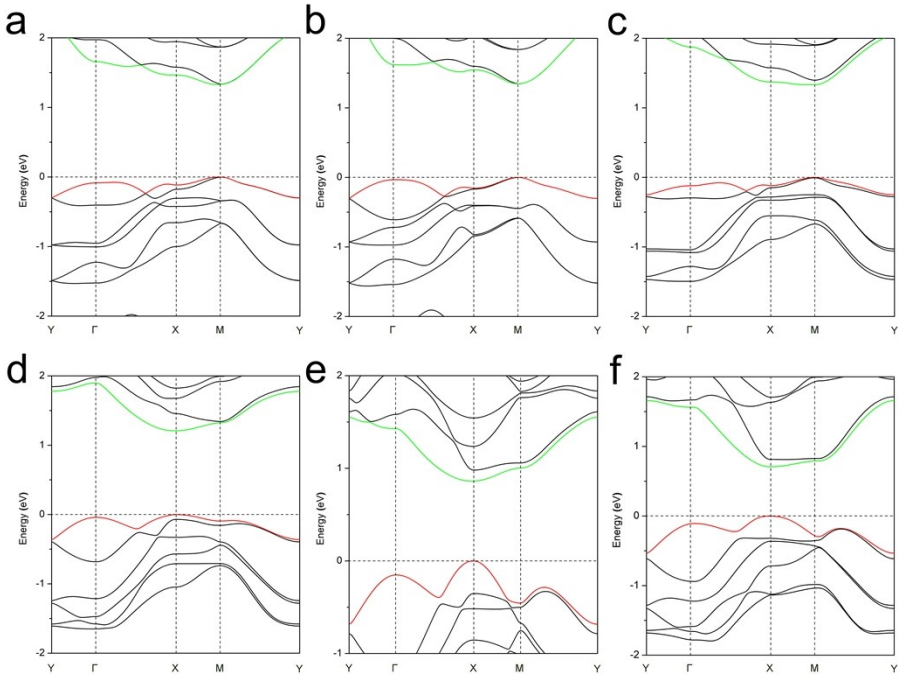

Figure S7. Band structures of the six different tellurenyne phases (PBE results). Figures (a)-(f) represent the phases from I to VI.

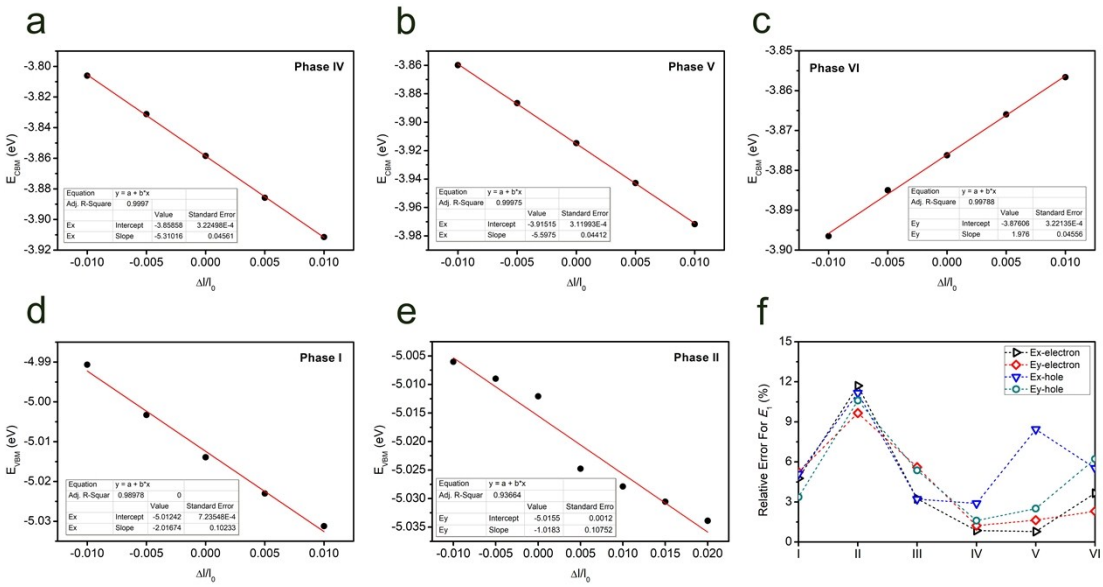

Figure S8. Representative relative errors for the defromation potential. The absolute energy changes of CBM under strain in phases IV, V and VI are shown in (a), (b) and (c); and the absolute energy changes of VBM

under strain in phases I and II are shown in (d) and (e). In (e), Two more data points at the tension strain of 1.5% and 2% are considered here to further reduce the fitting error of Ey-hole in phase II from 16.3% (five data points) to 10.6%. All the relative errors for the defromation potential in phases I to VI along x and y directions are shown in (f).

Table S2. Effective mass m^* (m_0), deformation potential E (eV), elastic module C (J/m^2) and carrier mobility μ (10^3 cm^2/V·s) of the six different tellurenyne phases along the transport directions (m_0 is the mass of the free electron).

Carrier	Phases	m^*_x	m^*_y	E_x	E_y	C_x	C_y	μ_x	μ_y
electron	I	1.84	0.30	4.31	0.27	18.72	8.96	0.016	12.045
	II	1.55	0.26	3.71	0.36	17.12	7.84	0.027	7.946
	III	0.30	0.49	5.54	0.66	18.56	7.68	0.113	2.042
	IV	0.29	1.02	5.31	1.58	18.40	8.16	0.087	0.125
	V	0.34	0.66	5.60	2.26	12.96	3.68	0.054	0.049
	VI	0.29	1.63	5.67	1.98	20.00	8.00	0.067	0.039
hole	I	0.79	0.36	2.02	1.51	18.72	8.96	0.238	0.442
	II	0.77	0.32	1.78	1.02	17.12	7.84	0.304	1.033
	III	0.66	0.44	1.14	1.45	18.56	7.68	0.859	0.328
	IV	0.23	0.90	0.95	1.89	18.40	8.16	4.083	0.118
	V	0.13	0.41	0.97	1.68	12.96	3.68	9.568	0.292
	VI	0.57	1.10	0.30	1.24	20.00	8.00	10.329	0.127